AGU100 ADVANCING EARTH AND SPACE SCIENCE

Geophysical Research Letters

RESEARCH LETTER
10.1002/2018GL077502

Key Points:
- The largest instrumentally recorded earthquake in the Pyrenees (M_w 5.4) corresponds to normal faulting at the south Pyrenean thrust front
- Earthquake distribution changes along strike of the chain, following the axial zone in the east and the mountain front in the west
- Western Pyrenean seismicity does not correlate with local gravitational potential energy, possibly due to stronger crust in this sector

Supporting Information:
- Data Set S1

Correspondence to:
D. Stich,
stich@ugr.es

Citation:
Stich, D., Martín, R., Batlló, J., Macià, R., Mancilla, F., & Morales, J. (2018). Normal faulting in the 1923 Berdún earthquake and postorogenic extension in the Pyrenees. *Geophysical Research Letters*, *45*, 3026–3034. https://doi.org/10.1002/2018GL077502

Received 7 FEB 2018
Accepted 14 MAR 2018
Accepted article online 25 MAR 2018
Published online 13 APR 2018

Normal Faulting in the 1923 Berdún Earthquake and Postorogenic Extension in the Pyrenees

Daniel Stich[1,2], Rosa Martín[1], Josep Batlló[3], Ramón Macià[4], Flor de Lis Mancilla[1,2], and Jose Morales[1,2]

[1]Instituto Andaluz de Geofísica, Universidad de Granada, Granada, Spain, [2]Departamento de Física Teórica y del Cosmos, Universidad de Granada, Granada, Spain, [3]Institut Cartogràfic i Geològic de Catalunya, Barcelona, Spain, [4]Departament de Matematiques, Universitat Politècnica de Catalunya, Barcelona, Spain

Abstract The 10 July 1923 earthquake near Berdún (Spain) is the largest instrumentally recorded event in the Pyrenees. We recover old analog seismograms and use 20 hand-digitized waveforms for regional moment tensor inversion. We estimate moment magnitude M_w 5.4, centroid depth of 8 km, and a pure normal faulting source with strike parallel to the mountain chain (N292°E), dip of 66° and rake of −88°. The new mechanism fits into the general predominance of normal faulting in the Pyrenees and extension inferred from Global Positioning System data. The unique location of the 1923 earthquake, near the south Pyrenean thrust front, shows that the extensional regime is not confined to the axial zone where high topography and the crustal root are located. Together with seismicity near the northern mountain front, this indicates that gravitational potential energy in the western Pyrenees is not extracted locally but induces a wide distribution of postorogenic deformation.

Plain Language Summary When convergence across a mountain chain comes to a stop, topography and deep root are no longer maintained, starting off postorogenic extension. Here we analyze the 10 July 1923 earthquake near Berdún in the Spanish Pyrenees. The earthquake was recorded at early analog seismographs over Europe, and we collected and hand digitized these old recordings for waveform analysis. We estimate moment magnitude M_w 5.4, making it the largest Pyrenean earthquake recorded on seismographs. The earthquake responds to normal faulting, indicating extension perpendicular to the mountain chain, in agreement with earthquakes in other parts of the Pyrenees, as well as deformation inferred from Global Positioning System data. It shows that postorogenic deformation reaches the southern mountain front, far from the largest topography and crustal root, which is at odds with conventional models for postorogenic extension.

1. Introduction

The Pyrenees formed as a collisional orogen between Europe and the formerly independent Iberian microplate, with main convergence during Eocene and Oligocene times (~55 to 25 Ma; e.g., Grool et al., 2018; Rosenbaum et al., 2002; Vergés et al., 2002). Since the early Miocene, Iberia shows no more relevant motion with respect to the rest of Europe, coincident with the slowing down of African-Eurasian convergence and the development of trench retreat and rollback in the Western Mediterranean area (Faccenna et al., 2014). Today, the level of seismicity in the Pyrenees is rather low, although major seismogenic structures have been identified in the chain (Alasset & Meghraoui, 2005; Ortuño et al., 2008), and moderate-size earthquakes with moment magnitude of ~5 occur occasionally (e.g., Batlló et al., 1997; Cara et al., 2008). Minor earthquakes take place along the entire length of the chain (e.g., Instituto Geográfico Nacional seismic catalog, Madrid; see Figure 1). The most relevant activity, regarding number and size of earthquakes, occurs at the French side of the western Pyrenees, along 80–100 km long, WNW-ESE lineament following approximately the trend of the North Pyrenean Fault. The major share of Pyrenees earthquakes occurs at shallow, upper crustal depths ($<$ 15 km), except for some deeper events (15 km to 40 km), mainly placed in the northwesternmost Pyrenees. Apart from natural seismicity, two distinct seismicity clusters have been related to subsidence at the Lacq gas field, in front of the northwestern Pyrenees (Segall et al., 1994), and the filling of the Itoiz reservoir in the southwestern Pyrenees (Ruiz et al., 2006; Santoyo et al., 2010).

Previous regional moment tensor, stress field, and Global Positioning System (GPS) studies (e.g., Chevrot et al., 2011; De Vicente et al., 2008; Serpelloni et al., 2007; Stich et al., 2006; Sylvander et al., 2008) paved

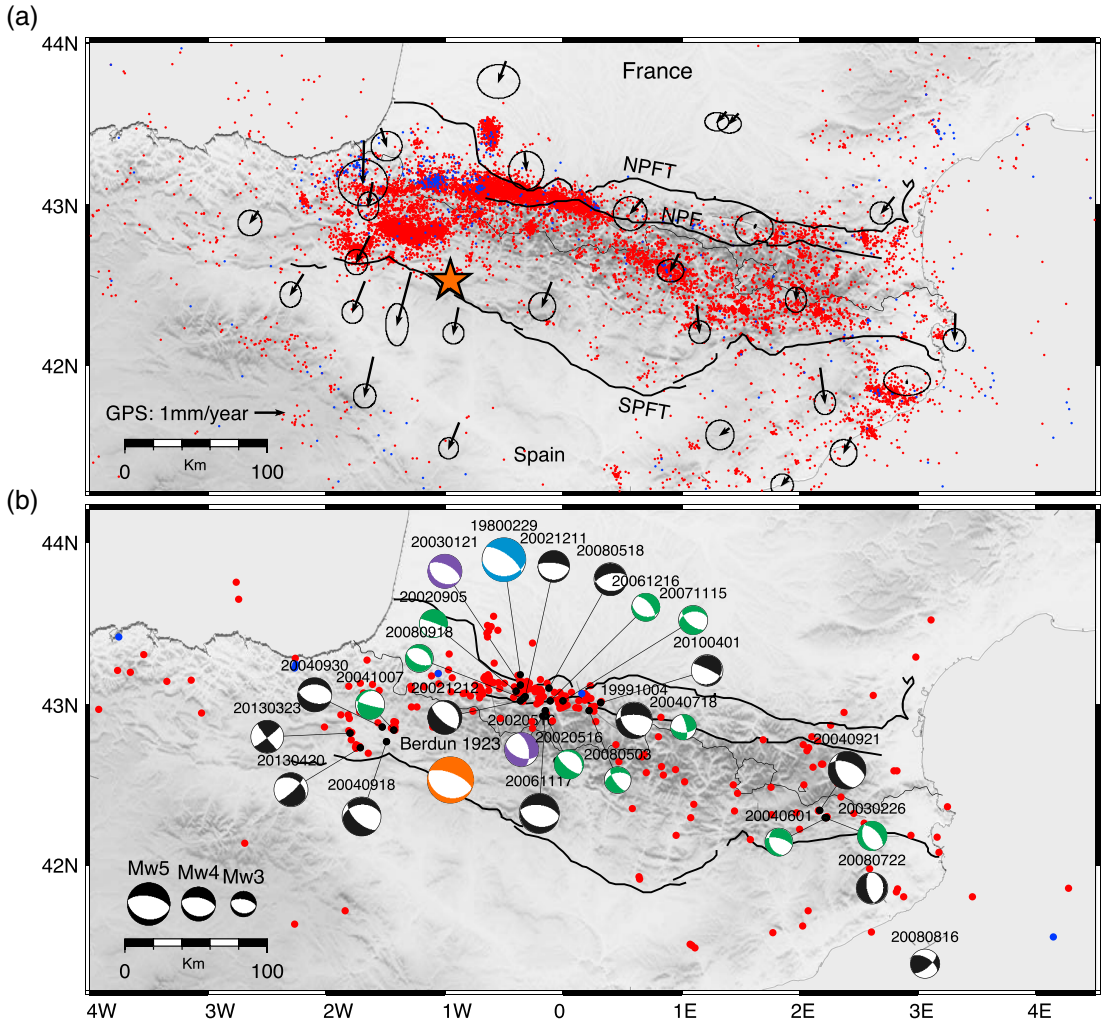

Figure 1. (a) Location map of the 1923 Berdún earthquake (star) with recent seismicity (from catalog of Instituto Geográfico Nacional, Madrid for years 1997–2016; depths less than 15 km are given in red, blue for depths from 15 to 40 km) and horizontal GPS velocities in Eurasia-fixed reference frame for continuous stations, along with 95% error ellipses (from Asensio et al., 2012, only stations with error less than 1 mm/year are represented). (b) The 1997–2016 earthquakes larger or equal magnitude 3 (Instituto Geográfico Nacional) and moment tensor solutions (double-couple component) provided by the IAG (Instituto Andaluz de Geofísica) catalog (black, Stich et al., 2003, 2006, 2010; Martín et al., 2015), Pyrenean catalog (green, Chevrot et al., 2011), ETH (Eidgenössische Technische Hochschule) catalog (purple, Braunmiller et al., 2002), and global CMT (Centroid Moment Tensor) catalog (blue, Dziewonski et al., 1981). Main tectonic structures NPFT, North Pyrenean Frontal Thrust; NPF, North Pyrenees fault; and SPFT, South Pyrenean Frontal Thrust (from Lacan & Ortuño, 2012).

the way to the idea that the Pyrenees double-vergent thrust belt is now subject to postcollisional extension. Various existing structures were reactivated as normal faults in present-day stress conditions (Lacan & Ortuño, 2012; Ortuño et al., 2008), and available earthquake moment tensor mechanisms show a clear predominance of normal faulting, with strike parallel to the chain (Braunmiller et al., 2002; Chevrot et al., 2011; Dziewonski et al., 1981; Martín et al., 2015; Stich et al., 2006, 2010; Figure 1). Postorogenic collapse of a mountain range is predicted when vertical gravitational forces from topography and crustal root are no longer compensated by active tectonic shortening (Molnar & Lyon-Caen, 1988). Besides gravity-induced stresses, diverse processes may contribute to postorogenic deformation in the Pyrenees, including rebound and uplift from denudation and deglaciation (Genti et al., 2016; Vernant et al., 2013), or deep-rooted thermal erosion in the easternmost part of the chain (Gunnell et al., 2008). Here we analyze an old earthquake in the southern Pyrenees, with remarkable size and singular location, and the way the results can contribute to advance our understanding of processes governing the present-day deformation in the chain.

Table 1
Source Estimates for the 1923 Berdún Earthquake

Time	Latitude (deg)	Longitude (deg)	z (km)	I_{max}	M	Reference
05:31:16.5	42.53	−0.95	36.4	-	-	Inglada (1929)
05:31:10.4	42.55	−0.95	20	VIII	-	Rey Pastor (1931).
05:31:13	42.5	−0.75	-	-	5.6	Gutenberg and Richter (1949)
05:31:10	42.5	−0.6	4	VIII	5.4	Munuera (1963)
05:31:12	42.6	−1.0	-	VIII	5.9	Karnik (1969)
05:31:10	42.5	−0.9	-	VIII	-	Suriñach and Roca (1982)
05:31:10.4	42.55	−0.95	-	VIII	-	Mezcua and Martínez Solares (1983)
05:31:--	42.63	−0.95	15	VII–VIII	5.8	Levret et al. (1996)
					6.3	
05:31:10	42.55	−0.95	-	VIII	5.7	Samardjieva et al. (1997)
					5.5	
--:--:--	42.55	−0.95	-	VIII	4.8	Badal et al. (2000)
--:--:--	42.63	−0.75	-	VIII	5.3	Mezcua et al. (2013)
	42.71	−0.87			5.5	

Note. Estimates for origin time (in format hour:minute:second), latitude, longitude, hypocentral depth, maximum macroseismic intensity, and magnitude published for the 1923 Berdún earthquake. Hyphens indicate that this value is not reported in the reference.

2. The 1923 Berdún Earthquake

On 10 July 1923, at 05:31 UTC, a major earthquake occurred in the foothills of the Aragonese Pyrenees (Spain), at a location quite remote from the main concentrations of recent seismicity in the chain (Figure 1). Two contemporary monographs (Inglada, 1929; Rey Pastor, 1931) provide detailed account of macroseismic effects and the wave arrival times at European seismograph stations, inferring an epicentral intensity Io = VIII and placing instrumental as well as macroseismic epicenter near the villages of Berdún and Martés (~42.55°N, 0.95°W). This situates the earthquake at ~10 km north of the south Pyrenean thrust front (Figure 1). Seismicity located at the mountain fronts is a typical expression of active orogens and remains intriguing in the case of the Pyrenees. Gutenberg and Richter (1949) assigned a first magnitude estimate ("d," equivalent to 5.6 ± 0.3), making this event a promising candidate for the largest-recorded Pyrenean earthquake. The contemporary epicenter location has been largely confirmed, within reasonable uncertainties, in subsequent catalogs (e.g., Levret et al., 1996; Mezcua et al., 2013; Munuera, 1963). Considerably larger uncertainties concern the magnitude, with reported estimates from records at single observatories ranging from M_w 4.8 (Badal et al., 2000) to M_s 6.3 (Levret et al., 1996), and other available macroseismic and instrumental magnitudes (Table 1) scattering between 5.3 and 5.9, in agreement with Gutenberg and Richter (1949).

The 1923 Berdún earthquake was recorded at a sparse network of early analog seismographs over Europe, and we will use seismic waveforms to infer the fault geometry for this earthquake. Original seismograms preserved in the archives from the observatories of Almeria, Coimbra, Piacenza, Strassbourg, and Toledo, together with the collection of seismograms in the Eurosismos database (Ferrari & Pino, 2003), provide recordings from 19 stations altogether. Based on dynamic range, frequency content, and general quality and stability of the recordings, we select a set of 20 seismograms from 9 observatories for further processing and regional waveform analysis (Figure 2). Most of these records are from Wiechert mechanical seismographs, except for two Bosch-Omori horizontal components at Almeria (Spain) and three components from electromagnetic Galitzin instruments at De Bilt (Netherlands). The vast majority of selected seismograms are obtained with horizontal sensors, superior in number among contemporary observatories equipment, and usually operating with longer free period in case of the prevailing mechanical sensors. All recordings were carefully hand digitized and corrected for drum speed, skew, and curvature of the traces and stylus instabilities (Batlló et al., 1997; Batlló, Stich, & Macià, 2008). We further compiled the accessible information on recording parameters, instrument design, and sensor orientations from bulletins and other documents, contemporary photos, annotations on paper seismograms, and on-site inspections, in order to estimate suitable transfer functions (compare Batlló, Stich, & Macià, 2008; Batlló, et al., 2010).

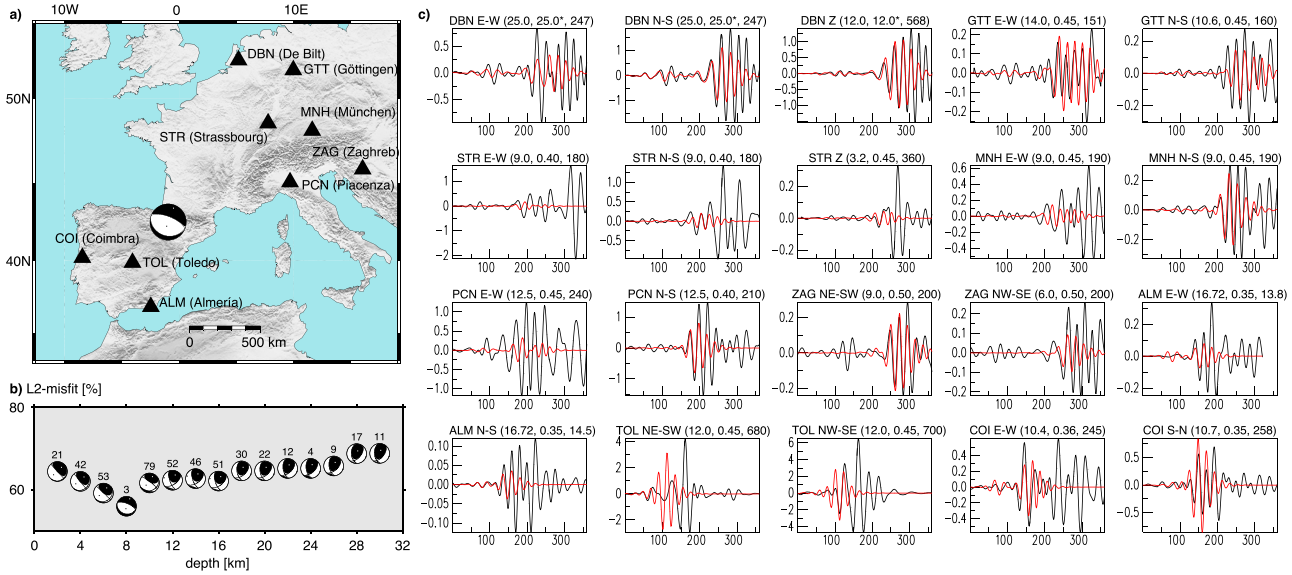

Figure 2. Moment tensor inversion for the 1923 Berdún earthquake, showing (a) station map and moment tensor solution, (b) fractional L2 misfit, moment tensor solutions and nondouble-couple component in percent (numbers above mechanisms) for different trial depths, and (c) waveform matches, sorted by stations azimuth, showing observed bandpass-filtered recordings (black) and synthetic predictions (red, including instrument response). Units are seconds and millimeter; *P* wave arrivals are aligned at 50 s. At all panels, the station code and component is labeled; number triplets in brackets give free period (s), damping, and amplification of the instrument. *For electromagnetic instruments (DBN), damping is critical, and the free period of the galvanometer (s) is given in place of the damping.

3. Moment Tensor Inversion

The digitized waveforms have been used for linear least squares moment tensor inversion. Specific problems related to the use of old seismograms were addressed by introducing two convenient modifications compared to standard regional moment tensor schemes: First, we process original horizontal seismograms individually, without rotation into a cylindrical ray-coordinate system (Stich et al., 2005). This avoids the propagation of recording instabilities, misalignments, or inaccurate instrument corrections into radial and transverse components. Second, we do not correct the instrument responses in the original recordings, but apply them to the Green's functions instead, to circumvent deconvolution for these old records (Batlló et al., 2010; Rivera et al., 2002). Further, we infer the unknown assignment of component orientation (E-W, N-S) to the Bosch-Omori recordings from Almeria by trial and error. Recorded waveforms and moment tensor Green's functions are filtered in an intermediate-period band (20 s to 50 s) that provides a reasonable compromise between the limited bandwidth of old sensors and an acceptable sensitivity of wave propagation to lateral heterogeneity in the lithosphere. Green's functions are computed with a reflectivity code and an average 1-D model for the Iberian lithosphere (Stich et al., 2003) that provides a suitable approximation also for wave propagation across most of western and central Europe (Stich et al., 2005). The nonlinear dependence of Green's functions on centroid depth is accommodated through a grid search for different trial depths between 2 km and 30 km, with step increment of 2 km.

We obtain a best fitting trial depth of 8 km (Figure 2), in agreement with the generally shallow origin of seismicity in the Pyrenees and the inner Iberian plate. Solutions for larger trial depths (centroid depth $\geq$ 12 km), showing a substantial rotation of the moment tensor (Figure 2), can be discarded on account of clear mismodeling for body waves. The depth range of largest variance reduction (6 km to 8 km) is located slightly deeper than the base of the Pyrenean edifice in the Berdún area (4 km to 5 km; Teixell, 1998), suggesting that the earthquake may be located below the basal thrust, within the autochthonous crust of the Iberian plate. Corresponding waveform matches are comparable to other regional inversion examples for old earthquakes (e.g., Batlló, Stich, Palombo, et al., 2008; Batlló et al., 2010; Stich et al., 2005) and are overall satisfactory in light of the characteristics of early instrumental records, the period band, and the propagation distances involved. Some amplitude misfit can be attributed to limited resolution from low dynamic and frequency range of the sensors, and uncertainties of the instrument response, like unstable damping (Batlló, Stich, & Macià, 2008), or

other discrepancies between actual recording parameters and estimated transfer functions. Large-amplitude pulses in the surface wave train (e.g., STR) may have been introduced by long-period disturbances, such as baseline instabilities. Waveform predictions are satisfactory at DBN and GTT, which represent particularly well-maintained instruments in direction of large Rayleigh wave radiation. We also adjust Love waves at MNH, PCN, and ZAG (NE and NW components), as well as amplitude and polarity of *P* waves at Iberian stations and DBN, while intermediate-period *P* waves are not resolved in recordings from other stations. Waveforms at ALM and COI are predicted reasonably, and we achieve a fair approximation to *P* waves in the NE component of TOL, as well as *S* waves in the NW component.

A double-couple contribution of 97% in the formally best moment tensor indicates that the Berdún earthquake can be modeled as simple shear faulting event. We infer pure normal faulting with the north dipping nodal planes oriented N292°E, 66°, −88° (strike, dip, and rake), and the south dipping nodal planes oriented N107°E, 24°, −94°. We lack further information to discriminate between fault and auxiliary plane, but we favor rupture on the steeper plane, showing a more typical dip value for crustal normal faulting earthquakes. The moment tensor T axes has strike of N20°E and plunge of 21°, indicating tension perpendicular to the Pyrenees. We obtain scalar seismic moment $M_0 = 1.5 \times 10^{17}$ Nm, equivalent to moment magnitude M_w 5.4. In comparison with estimated moment magnitudes for other major Pyrenean earthquakes, this ranks the 1923 Berdún earthquake as the largest instrumental event so far: It was slightly larger than the 19 November 1923, M_w 5.3 earthquake in the Aran Valley (Batlló et al., 1997; Susagna et al., 1994), and clearly larger than the 13 August 1967, M_w 5.1 Arette earthquake (Cara et al., 2008) and the M_w 5.1, 1980 Arudy earthquake (Dziewonski et al., 1981).

4. Present-Day Deformation and Potential Energy

The obtained moment tensor gives new clues for postorogenic extension in the Pyrenees. Normal faulting for the 1923 Berdún earthquake agrees with faulting style and orientation from moment tensors for more recent Pyrenean earthquakes (Figure 1b). Moreover, due to its size and solitary location, this event consolidates substantially the idea of present-day extension perpendicular to the chain. In particular, it shows that also the realm of the southern frontal thrust of the western Pyrenees is now subject to normal faulting under tensional stress. This resembles the situation on the other side of the chain, where normal faulting occurs in the vicinity of the northwestern mountain front. Present-day extension across the full width of the western Pyrenees is in agreement with the regional velocity fields from GPS data (Figure 1a). While no significant horizontal strain has been resolved in the eastern Pyrenees, GPS data from continuous network stations lead to estimates for extensional strain across the western Pyrenees in NNW-SSE direction, with rates from ~2.5 nanostrain per year (Asensio et al., 2012) to ~4 nanostrain per year (Nguyen et al., 2016). The results are similar to estimates from campaign data (~2 nanostrain per year, Rigo et al., 2015). Vertical GPS velocities are not resolved (~0.1 ± 0.2 mm/year, Nguyen et al., 2016), although the small value might solely reflect the net effect due to subsidence from gravitation and uplift from erosional denudation.

General models for gravity-driven postorogenic extension predict tension perpendicular to the chain, and associated extensional faulting, in the axial zone of mountain ranges, while compression should occur in the foothills (Molnar & Lyon-Caen, 1988). Rebound from erosion and deglaciation is related to topography in an analogous way and induces a similar pattern of extension and compression in the upper crust (Sue et al., 2007; Vernant et al., 2013). Hence, the 1923 Berdún earthquake, as well as the other recent earthquakes associated to the same type of faults in the frontal areas of the northwestern Pyrenees, occurs in settings where thrust faulting would be expected a priori (Chevrot et al., 2014; Genti et al., 2016). To investigate the influence of topography and crustal root on the seismicity pattern, we estimate local gravitational potential energy of the crust, per unit area, according to equation (2) in Molnar and Lyon-Caen (1988). We report relative values, comparing the potential energy density to a reference crust with elevation of 0 m above sea level and Moho depth of 30 km. A smooth Moho topography for modeling has been interpolated from available receiver function measurements (Mancilla & Diaz, 2015). Isostacy is not imposed, and we assume constant crustal density of 2,800 kg/m^3 and a signed crust-mantle density contrast of ±500 kg/m^3 throughout, with positive and negative contrasts associated to local Moho below or above the reference Moho depth. The obtained map of gravitational potential energy density is dominated by the signal from topography (Figure 3) and does not suggest relevant tensional strain at the location of the 1923 Berdún earthquake.

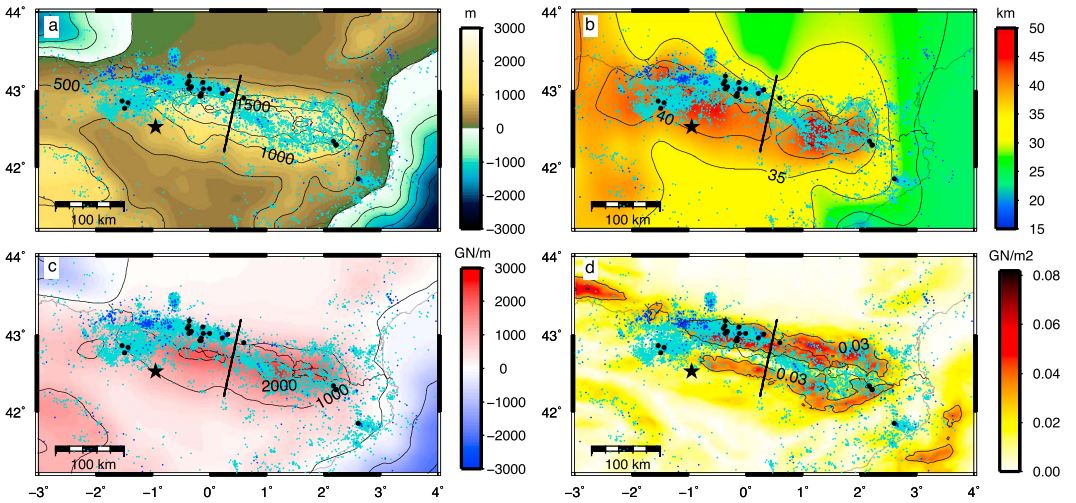

Figure 3. Relationship of seismicity (1997–2016, Instituto Geográfico Nacional, depths less than 15 km in light blue, depths deeper 15 in dark blue), with (a) filtered topography, (b) crustal thickness (from Mancilla & Diaz, 2015), (c) potential energy per unit area (in 10^9 N/m), defined as work against gravity stored in topography and crustal root (Molnar & Lyon-Caen, 1988), and (d) the value of the gradient vector of potential energy density (in 10^9 N/m^2). Magnitudes of all parameters are shown through labeled contour lines. The straight line at ~0.5°E separates different patterns in the western and eastern Pyrenees. Black dots indicate earthquakes with available normal faulting moment tensors, and the star marks the 1923 earthquake.

5. Discussion

From the results obtained in previous sections, it is now clear that the largest recorded Pyrenean earthquake is located near the southern thrust front of the belt and corresponds to pure normal faulting. It emphasizes the presence of widespread extension across the western Pyrenees. Normal faults are active also in central Iberia (Martín et al., 2015), so, in principle, normal faulting beneath the Pyrenean mountain front could be driven by regional stresses and occur despite of, not because of, postorogenic extension of the chain. On the other hand, a dominant role of local stresses is suggested by the alignment between the strike of the chain, strike of normal faulting mechanisms, and stress tensor in the western Pyrenees (σ_2 at N110°E, Rigo et al., 2015), introducing a ~25° rotation of the Pyrenean stress field with respect to central Iberia (De Vicente et al., 2008). Comparing the distribution of Pyrenean seismicity to gravitational potential energy density (Figure 3), we appreciate irregular correlation among them. In particular, we can identify a clear change in the pattern along strike of the Pyrenees: East of ~0.5°E longitude, earthquakes are concentrated in the axial zone, coincident with maximum gravitational potential energy, while west of this point, seismicity spreads out over the entire width of the chain, and a major part of events concentrate in the frontal zones (in particular, on the northern side), coincident with the largest lateral gradients of potential energy (Figure 3d). Beyond this dichotomous first-order pattern, seismicity becomes more distributed at the eastern and western terminations of the mountain belt (including the superposition of induced seismicity on the western side).

Along-strike variations in seismicity are also reflected in focal mechanisms and stress tensor estimates (Goula et al., 1999; Rigo et al., 2015). Extensional processes in the western Mediterranean affect the easternmost Pyrenees, featuring active graben faults and recent anorogenic volcanism (e.g., Vergés et al., 2002), thermal erosion of the lithospheric root, and Neogene uplift (Gunnell et al., 2008). The sharp transition between the contrasting seismicity patterns near 0.5°E, however, makes a far-field origin like the removal of mantle lithosphere less conceivable, pointing to a control by local agents. We suggest variations in crustal strength as the decisive factor. Gravitational potential energy is a local concept that may correlate with deformation for low crustal strength, while stronger material may respond by flexure and may transfer stresses away from their local buoyancy or topography source. Different rheology in western and eastern Pyrenees has been proposed previously (e.g., Jammes et al., 2014; McClay et al., 2004), since deep seismic surveys show the emplacement of thin and highly deformed thrust sheets in the eastern Pyrenees (Grool et al., 2018; Muñoz, 1992), compared to much thicker and less deformed thrust sheets in the western Pyrenees (Teixell, 1998).

These differences have been attributed to inherited crustal composition of the Paleozoic basement (García-Sansegundo et al., 2011; Jammes et al., 2014), showing an overall weaker and more felsic crust in the eastern part, representing the Variscan hinterland, as compared to overall stronger and more mafic crust in the western part, originating from the Variscan foreland domain. Note that the foreland-hinterland boundary trends obliquely to the chain, and surface exposure of Variscan intrusive rocks becomes gradually less abundant from east to west (García-Sansegundo et al., 2011; Lacan & Ortuño, 2012). Alternatively, the along-strike variation in strength may be influenced by the abundance and distribution of mechanically weak Triassic evaporites (McClay et al., 2004).

Based on clear changes along strike in the internal structure of the Pyrenees, the bulk strength of the crust is expected to decrease from east to west and appears to reach a tipping point near 0.5°E, where a sharp contrast in the seismicity distribution is located. In this scenario, within the mechanically weak eastern Pyrenees, seismicity correlates with gravitational potential energy, including relevant earthquakes in the axial zone like the 1923, M_w 5.3, Aran Valley event (Ortuño et al., 2008). The local response of the crust prevents net extension across the chain but may be an ingredient to the relevant heterogeneity of first motion earthquake focal mechanisms (Goula et al., 1999; Rigo et al., 2015). In fact, these authors provide evidence for the coexistence of compressional and extensional stress fields in immediate proximity and short wavelength anomalies in GPS velocities for the eastern part of the range. In the presumably stronger material of the western Pyrenees crust, the response to gravitational forces may occur on much wider areas (Genti et al., 2016), and deformation is transferred to the external part of the chain. This results in an extensional signature in the regional GPS strain field (Nguyen et al., 2016), as well as relevant normal faulting earthquakes near the external thrusts on both sides of the chain, as is demonstrated for the South Pyrenean Frontal Thrust by the 1923 Berdún earthquake.

Acknowledgments

We are grateful to all the individuals and institutions committed to the preservation and distribution of old analog seismograms. The constructive comments from Giorgi Khazaradze and an anonymous reviewer helped to improve the manuscript. We used free software SAC (Goldstein et al., 2003) and GMT (Wessel & Smith, 1998). Digitized waveforms in SAC format are provided as supporting information. We received financial support through Mineco/Feder Project CGL2015-67130-C2-2-R, PP2012-PIJD003 from Granada University, and Junta de Andalucía research group RNM 104.

References

Alasset, P. J., & Meghraoui, M. (2005). Active faulting in the Western Pyrenees (France): paleoseismic evidence for Late Holocene ruptures. *Tectonophysics*, *409*, 39–54. https://doi.org/10.1016/j.tecto.2005. 08.019

Asensio, E., Khazaradze, G., Echeverria, A., King, R. W., & Vilajosana, I. (2012). GPS studies of active deformation in the Pyrenees. *Geophysical Journal International*, *190*, 913–921. https://doi.org/10.1111/j.1365-246X.2012.05525

Badal, J., Samardjieva, E., & Payo, G. (2000). Moment magnitude for early (1923–1961) instrumental Iberian earthquakes. *Bulletin of the Seismological Society of America*, *90*(5), 1161–1173. https://doi.org/10.1785/0119990146

Batlló, J., Stich, D., & Macià, R. (2008). Quantitative analysis of early seismograph recordings. In J. Fréchet, M. Meghraoui, & M. Stucchi (Eds.), *Historical seismology* (pp. 385–402). Dordrecht: Springer. https://doi.org/10.1007/978-1-4020-8222-1_19

Batllo, J., Stich, D., Macia, R., & Morales, J. (2010). Moment tensor inversion for the 5 July 1930 Montilla earthquake (southern Spain). *Seismological Research Letters*, *81*(5), 724–731. https://doi.org/10.1785/gssrl.81.5.724

Batlló, J., Stich, D., Palombo, B., Macia, R., & Morales, J. (2008). The 1951 M_w 5.2 and M_w 5.3 Jaén, southern Spain, earthquake doublet revisited. *Bulletin of the Seismological Society of America*, *98*(3), 1535–1545. https://doi.org/10.1785/%200120070038

Batlló, J., Susagna, T., & Roca, A. (1997). A processing system for old records of regional earthquakes: Analysis of the 19 November 1923 earthquake in the Pyrenees. *Cahiers du Centre Européen de Géodynamique et de Séismologie*, *13*, 159–175.

Braunmiller, J., Kradolfer, U., Baer, M., & Giardini, D. (2002). Regional moment tensor determination in the European-Mediterranean area: Initial results. *Tectonophysics*, *356*(1-3), 5–22. https://doi.org/10.1016/S0040-1951(02)00374-8

Cara, M., Alasset, P. J., & Sira, C. (2008). Magnitude of historical earthquakes, from macroseismic data to seismic waveform modelling: Application to the Pyrenees and a 1905 earthquake in the Alps. In J. Fréchet, M. Meghraoui, & M. Stucchi (Eds.), *Historical seismology* (pp. 369–384). Dordrecht: Springer. https://doi.org/10.1007/978-1-4020-8222-1_18

Chevrot, S., Sylvander, M., & Delouis, B. (2011). A preliminary catalog of moment tensors for the Pyrenees. *Tectonophysics*, *510*(1-2), 239–251. https://doi.org/10.1016/j.tecto.2011.07.011

Chevrot, S., Villaseñor, A., Sylvander, M., Benahmed, S., Beucler, E., Cougoulat, G., et al. (2014). High-resolution imaging of the Pyrenees and massif central from the data of the PYROPE and IBERARRAY portable array deployments. *Journal of Geophysical Research: Solid Earth*, *119*, 6399–6420. https://doi.org/10.1002/2014JB010953

De Vicente, G., Cloetingh, S., Muñoz-Martín, A., Olaiz, A., Stich, D., Vegas, R., et al. (2008). Inversion of moment tensor focal mechanisms for active stresses around the microcontinent Iberia: Tectonic implications. *Tectonics*, *27*, TC1009. https://doi.org/10.1029/2006TC002093

Dziewonski, A. M., Chou, T. A., & Woodhouse, J. H. (1981). Determination of earthquake source parameters from waveform data for studies of global and regional seismicity. *Journal of Geophysical Research*, *86*(B4), 2825–2852. https://doi.org/10.1029/JB086iB04p02825

Faccenna, C., Becker, T. W., Auer, L., Billi, A., Boschi, L., Brun, J. P., et al. (2014). Mantle dynamics in the Mediterranean. *Reviews of Geophysics*, *52*, 283–332. https://doi.org/10.1002/%202013RG000444

Ferrari, G., & Pino, N. A. (2003). Euroseismos 2002–2003, a project for saving and studying historical seismograms in the Euro-Mediterranean área. *Geophysical Research Abstracts*, *5*, 05274.

García-Sansegundo, J., Poblet, J., Alonso, J. L., & Clariana, P. (2011). Hinterland-foreland zonation of the Variscan orogen in the central Pyrenees: Comparison with the northern part of the Iberian Variscan massif. *Geological Society of London, Special Publications*, *349*(1), 169–184. https://doi.org/10.1144/%20SP349.9

Genti, M., Chery, J., Vernant, P., & Rigo, A. (2016). Impact of gravity forces and topography denudation on normal faulting in central–western Pyrenees: Insights from 2D numerical models. *Comptes Rendus Geosciences*, *348*(3-4), 173–183. https://doi.org/10.1016/j.crte.% 202015.08.004

Goldstein, P., Dodge, D., Firpo, M., & Minner, L. (2003). *SAC2000: Signal processing and analysis tools for seismologists and engineers. IASPEI International Handbook of Earthquake and Engineering Seismology*. Amsterdam & Boston: Academic Press.
Goula, X., Olivera, C., Fleta, J., Grellet, B., Lindo, R., Rivera, L. A., et al. (1999). Present and recent stress regime in the eastern part of the Pyrenees. *Tectonophysics*, *308*(4), 487–502. https://doi.org/10.1016/S0040-1951(99)00120-1
Grool, A. R., Ford, M., Vergés, J., Huismans, R. S., Christophoul, F., & Dielforder, A. (2018). Insights into the crustal-scale dynamics of a doubly vergent orogen from a quantitative analysis of its forelands: A case study of the eastern Pyrenees. *Tectonics*, *37*, 450–476. https://doi.org/10.1002/2017TC004731
Gunnell, Y., Zeyen, H., & Calvet, M. (2008). Geophysical evidence of a missing lithospheric root beneath the eastern Pyrenees: Consequences for post-orogenic uplift and associated geomorphic signatures. *Earth and Planetary Science Letters*, *276*(3-4), 302–313. https://doi.org/10.1016/j.epsl.2008.09.031
Gutenberg, B., & Richter, C. F. (1949). *Seismicity of the Earth and associated phenomena*. Princeton: Princeton University Press.
Inglada Ors, V. (1929). Contribución al estudio del sismo pirenaico (Canal de Berdún) de 10 de julio 1923. *Revista de la Real Academia de Ciencias Exactas, Físicas y Naturales, de Madrid*, *24*, 448–501.
Jammes, S., Huismans, R. S., & Muñoz, J. A. (2014). Lateral variation in structural style of mountain building: Controls of rheological and rift inheritance. *Terra Nova*, *26*(3), 201–207. https://doi.org/10.1111/ter.12087
Karnik, V. (1969). *Seismicity of the European area* (Vol. 1, p. 364). Dordrecht, Holland: D. Reidel Co.
Lacan, P., & Ortuño, M. (2012). Active tectonics of the Pyrenees: A review. *Journal of Iberian Geology*, *38*, 9–30. https://doi.org/10.5209/rev_JIGE.2012.v38.n1.39203
Levret, A., Cushing, M., & Peyridieu, G. (1996). Recherche des caractéristiques de séismes historiques en France. Atlas de 140 cartes macrosismiques. Publication IPSN, 2 vol., 400p. et 140 cartes.
Mancilla, F., & Diaz, J. (2015). High resolution Moho topography map beneath Iberia and northern Morocco from receiver function analysis. *Tectonophysics*, *663*, 203–211. https://doi.org/10.1016/j.tecto.2015.06.017
Martín, R., Stich, D., Morales, J., & Mancilla, F. (2015). Moment tensor solutions for the Iberian-Maghreb region during the Iberarray deployment. *Tectonophysics*, *663*, 261–274. https://doi.org/10.1016/j.tecto.2015.08.012
McClay, K., Muñoz, J. A., & García Sanz, J. (2004). Extensional salt tectonics in a contractional orogen: A newly identified tectonic event in the Spanish Pyrenees. *Geology*, *32*(9), 737–740. https://doi.org/10.1130/G20565
Mezcua, J., & Martínez Solares, J. M. (1983). Sismicidad del área Iberomogrebi. Instituto Geográfico Nacional. Pub. 203 (301 pp.).
Mezcua, J., Rueda, J., & García Blanco, R. M. (2013). Iberian peninsula historical seismicity revisited: An intensity data bank. *Seismological Research Letters*, *84*(1), 9–18. https://doi.org/10.1785/0220120097
Molnar, P., & Lyon-Caen, H. (1988). Some simple physical aspects of the support, structure, and evolution of mountain belts. *Geological Society of America Special Papers*, *218*, 179–207. https://doi.org/10.1130/SPE218-p179
Muñoz, J. A. (1992). Evolution of a continental collision belt: ECORS-Pyrenees crustal balanced cross-section. In K. R. McClay (Ed.), *Thrust tectonics* (pp. 235–246). Dordrecht: Springer. https://doi.org/10.1007/978-94-011-3066-0_21
Munuera, J. M. (1963). A study of seismicity on the península Ibérica area. Technical note n.1 'Seismic data.' Inst. Geográfico y Catastral (93 pp.).
Nguyen, H., Vernant, P., Mazzotti, S., Khazaradze, G., & Asensio, E. (2016). 3-D GPS velocity field and its implications on the present-day post-orogenic deformation of the western Alps and Pyrenees. *Solid Earth*, *7*(5), 1349–1363. https://doi.org/10.5194/se-7-1349-2016
Ortuño, M., Queralt, P., Martì, A., Ledo, J., Masana, E., Perea, H., & Santanach, P. (2008). The north Maladeta fault (Spanish central Pyrenees) as the Vielha 1923 earthquake seismic source: Recent activity revealed by geomorphological and geophysical research. *Tectonophysics*, *453*(1-4), 246–262. https://doi.org/10.1016/j.tecto.2007.06.016
Rey Pastor, A. (1931). *El periodo sísmico de la Canal de Berdún, Pirineos (1923–1925)*. Toledo: Instituto Geográfico y Catastral.
Rigo, A., Vernant, P., Feigl, K. L., Goula, X., Khazaradze, G., Talaya, J., et al. (2015). Present-day deformation of the Pyrenees revealed by GPS surveying and earthquake focal mechanisms until 2011. *Geophysical Journal International*, *201*(2), 947–964. https://doi.org/10.1093/gji/ggv052
Rivera, L., Sieh, K., Helmberger, D., & Natawidjaja, D. (2002). A comparative study of the Sumatran subduction-zone earthquakes of 1935 and 1984. *Bulletin of the Seismological Society of America*, *92*(5), 1721–1736. https://doi.org/10.1785/0120010106
Rosenbaum, G., Lister, G. S., & Duboz, C. (2002). Relative motions of Africa, Iberia and Europe during Alpine orogeny. *Tectonophysics*, *359*(1-2), 117–129. https://doi.org/10.1016/S0040-1951(02)00442-0
Ruiz, M., Gaspà, O., Gallart, J., Díaz, J., Pulgar, A. A., García-Sansegundo, J., et al. (2006). Aftershocks series monitoring of the September 18, 2004 $M = 4.6$ earthquake at the western Pyrenees: A case of reservoir-triggered seismicity? *Tectonophysics*, *424*(3-4), 223–243. https://doi.org/10.1016/j.tecto.2006.03.037
Samardjieva, E., Payo, G., & Badal, J. (1997). *Catalogue of digital historical seismograms (1912–1962). Wiechert seismograph, geophysical observatory of Toledo* (306 pp.). Madrid: Instituto Geografico Nacional.
Santoyo, M. A., García-Jerez, A., & Luzón, F. (2010). A subsurface stress analysis and its possible relation with seismicity near the Itoiz reservoir, Navarra, northern Spain. *Tectonophysics*, *482*(1-4), 205–215. https://doi.org/10.1016/j.tecto.2009.06.022
Segall, P., Grasso, J. R., & Mossop, A. (1994). Poroelastic stressing and induced seismicity near the Lacq gas field, southwestern France. *Journal of Geophysical Research*, *99*(B8), 15,423–15,438. https://doi.org/10.1029/94JB00989
Serpelloni, E., Vannucci, G., Pondrelli, S., Argnani, A., Casula, G., Anzidei, M., et al. (2007). Kinematics of the western Africa–Eurasia plate boundary from focal mechanisms and GPS data. *Geophysical Journal International*, *169*(3), 1180–1200. https://doi.org/10.1111/j.1365-246X.2007.03367.x
Stich, D., Ammon, C. J., & Morales, J. (2003). Moment tensor solutions for small and moderate earthquakes in the Ibero-Maghreb region. *Journal of Geophysical Research*, *108*(B3), 2148. https://doi.org/10.1029/2002JB002057
Stich, D., Batlló, J., Macià, R., Teves-Costa, P., & Morales, J. (2005). Moment tensor inversion with single-component historical seismograms: The 1909 Benavente (Portugal) and Lambesc (France) earthquakes. *Geophysical Journal International*, *162*(3), 850–858. https://doi.org/10.1111/j.1365-246X.2005.02680.x
Stich, D., Martin, R., & Morales, J. (2010). Moment tensor inversion for Iberia-Maghreb earthquakes 2005–2008. *Tectonophysics*, *483*(3-4), 390–398. https://doi.org/10.1016/j.tecto.2009.11.006
Stich, D., Serpelloni, E., Mancilla, F., & Morales, J. (2006). Kinematics of the Iberia-Maghreb plate contact from seismic moment tensors and GPS observations. *Tectonophysics*, *426*(3-4), 295–317. https://doi.org/10.1016/j.tecto.2006.08.004
Sue, C., Delacou, B., Champagnac, J. D., Allanic, C., Tricart, P., & Burkhard, M. (2007). Extensional neotectonics around the bend of the western/central Alps: An overview. *International Journal of Earth Sciences*, *96*(6), 1101–1129. https://doi.org/10.1007/s00531-007-0181-3
Suriñach, E., & Roca, A. (1982). Catálogo de Terremotos de Cataluña, Pirineos y zonas adyacentes, 1100-1979. *Universidad Complutense, Cátedra de Geofísica, Publicación Técnica*, *190*, 9–106.

Susagna, T., Roca, A., Goula, X., & Batlló, J. (1994). Analysis of macroseismic and instrumental data for the study of the 19 November 1923 earthquake in the Aran Valley (central Pyrenees). *Natural Hazards*, *10*(1-2), 7–17. https://doi.org/10.1007/BF00643438

Sylvander, M., Souriau, A., Rigo, A., Tocheport, A., Toutain, J. P., Ponsolles, C., & Benahmed, S. (2008). The 2006 November, *ML* = 5.0 earthquake near Lourdes (France): New evidence for NS extension across the Pyrenees. *Geophysical Journal International*, *175*(2), 649–664. https://doi.org/10.1111/j.1365-246X.2008.03911.x

Teixell, A. (1998). Crustal structure and orogenic material budget in the west central Pyrenees. *Tectonics*, *17*(3), 395–406. https://doi.org/10.1029/98TC00561

Vergés, J., Fernàndez, M., & Martínez, A. (2002). The Pyrenean orogen: Pre-, syn-, and postcollisional evolution. *Journal of the Virtual Explorer*, *08*, 55–74. https://doi.org/10.3809/jvirtex.2002.00058

Vernant, P., Hivert, F., Chéry, J., Steer, P., Cattin, R., & Rigo, A. (2013). Erosion-induced isostatic rebound triggers extension in low convergent mountain ranges. *Geology*, *41*(4), 467–470. https://doi.org/10.1130/G33942.1

Wessel, P., & Smith, W. H. F. (1998). New, improved version of the Generic Mapping Tools released. *Eos, Transactions American Geophysical Union*, *79*(47), 579. https://doi.org/10.1029/98EO00426